International Journal for Computational Methods in Engineering Science and Mechanics
Publication details, including instructions for authors and subscription information:
http://www.informaworld.com/smpp/title~content=t713872093

Numerical Simulation of 3-D Potential Problems by Regular Hybrid Boundary Node Method

Jianming Zhang [a]
[a] College of Mechanical and Automotive Engineering, Hunan University, Changsha, China

Online Publication Date: 01 March 2008
To cite this Article: Zhang, Jianming (2008) 'Numerical Simulation of 3-D Potential Problems by Regular Hybrid Boundary Node Method', International Journal for Computational Methods in Engineering Science and Mechanics, 9:2, 111 - 120
To link to this article: DOI: 10.1080/15502280701815390
URL: http://dx.doi.org/10.1080/15502280701815390

International Journal for Computational Methods in Engineering Science and Mechanics, 9:111–120, 2008

ISSN: 1550–2287 print / 1550–2295 online
DOI: 10.1080/15502280701815390

Numerical Simulation of 3-D Potential Problems by Regular Hybrid Boundary Node Method

Jianming Zhang
College of Mechanical and Automotive Engineering, Hunan University, Changsha, China

The Regular Hybrid Boundary Node Method (RHBNM) is developed for solving three-dimensional potential problems. Formulations are developed and a general computer code written in C++. The RHBNM is formulated in terms of the domain and boundary variables. The domain variables are interpolated by classical fundamental solutions with the source points located outside the domain, and the boundary variables are interpolated by MLS approximation. The main idea is to retain the dimensionality advantages of the Boundary Element Method, and localize the integration domain to a regular sub-domain so that no mesh is needed for integration. All integrals can be easily evaluated over regularly shaped domains (in general, semi-sphere in the 3-D problem) and their boundaries. Numerical examples demonstrate that high convergence rate with mesh refinement and high accuracy with a small node number are achievable.

Keywords Meshless Method, Moving Least-Squares Approximation, Hybrid Boundary Node Method, Potential Problem

1. INTRODUCTION

Although the Finite Element Method (FEM) and Boundary Element Method (BEM) have made great achievements in solving practical engineering problems, the interest of pursuing new methods has never decreased through time. This is because, with mesh-based techniques, the task of mesh generation for complex geometries is often time-consuming and prone to errors, and the difficulties with re-meshing in problems involving moving boundaries, large deformations or crack propagation are enormous, in spite of significant progress made in 3-D meshing algorithms. In recent years, novel algorithms, referred to as "meshless" methods, have been proposed that largely circumvent the problems associated with meshing.

Meshless methods originate from the Smooth Particle Hydrodynamics (SPH) method for modeling astrophysical phenomena [1], and gain popularity after the publication of the diffuse element method [2] and the element free Galerkin method (EFG) [3]. The EFG uses a global symmetric weak form and the shape functions from the moving least-squires approximation. Although no mesh is required for the variable interpolation, background cells are inevitable for the "energy" integration. Therefore, the EFG method is a pseudo-meshless method.

To avoid the use of the background cells and thus achieve a truly meshless method, Atluri and his co-workers have introduced a Meshless Local Boundary Integral Equation (MLBIE) [4] and a Meshless Local Petrov-Galerkin (MLPG) approach [5]. Both methods use local weak forms over a local sub-domain, and therefore are truly meshless, as no "finite element or boundary element mesh" is required either for the variable interpolation or for the "energy" integration. All integrals can be easily evaluated over regularly shaped domains (for example, circles in 2-D problems and spheres in 3-D problems) and their boundaries.

In 1997, Mukherjee et al. proposed a boundary-type meshless method, which they call the Boundary Node Method (BNM) [6]. The BNM combines the MLS interpolants with Boundary Integral Equations (BIE) in order to retain both the meshless attribute of the former and the dimensionality advantage of the latter. This method only requires a nodal data structure on the bounding surface of a body. However, this method is still not a truly meshless one, as an underlying cell structure is again used for boundary integration.

A question arises here—is there possibly a method of solving boundary value problems that only requires nodes constructed on the surface of a domain and requires no cells either for interpolation of the solution variables or for the numerical integration? This method will essentially simplify the input data structure, and be an important step in the direction towards complete analysis automation.

The answer is positive. One of the possibilities can be the Hybrid Boundary Node Method (Hybrid BNM) [7], which combines the MLS interpolation scheme with the hybrid displacement variational formulation. However, the Hybrid BNM has a

Received 1 March 2007; in final form 23 October 2007.
This work is supported by the national 973 program under grant number 2004CB719402 and the program for New Century Excellent Talents in University (NCET-04-0766).
Address correspondence to Jianming Zhang, College of Mechanical and Automotive Engineering, Hunan University, Changsha 410082, China. E-mail: zhangjianm@gmail.com

drawback of serious "boundary layer effect," i.e. the accuracy of results in the vicinity of the boundary is sensitive to the proximity of the interior points to the boundary. To overcome this problem, a new Regular Hybrid Boundary Node Method (RHBNM) was proposed by the same authors [8–10]. In the new method, the source points of the fundamental solutions are located outside the domain rather than on the boundary as in the Hybrid BNM or other hybrid boundary element models [11, 12]. Computations for 2-D potential problems show that the numerical results are no more sensitive to the proximity of the interior points to the boundary. Very high accuracy can be achieved with a small number of boundary nodes. In this paper, the RHBNM is further developed for solving 3-D potential problems.

The hybrid boundary element method was first proposed by Schnack [13], in which he stressed using the boundary element method to generate a hybrid stress finite element model, giving rapid convergence of the results and accurate solution for stress concentration problems. Dumont [11] has presented a hybrid stress boundary element formulation based on Hellinger-Reissner principle with stresses in the domain and displacements on the boundary as independent functions. DeFigueredo and Brebbia [12] have introduced a hybrid displacement variational formulation of BEM, which is based on a modified functional using three independent variables, i.e. displacements and tractions on the boundary and displacements inside the domain. This approach uses the classical fundamental solution to interpolate the displacements in the domain and thus allowing for the transfer of the domain integrals to the boundary. The resulting system of equations is written in terms of boundary displacements only, and has the advantage of being symmetrical, which is easy to couple with the FEM. In the present paper, the objective is not to obtain the symmetrical system of equations, but a truly boundary-type meshless method by combining the hybrid displacement variational formulation and the meshless interpolation scheme. The variables on the boundary are interpolated by MLS scheme and a truly meshless RHBNM is achieved.

The following discussion begins with the brief description of the MLS approximation in Section 2. The formulation of RHBNM for 3-D potential problems is developed in Section 3. Numerical examples for 3-D potential problems are given in Section 4. The paper ends with conclusions and discussions in Section 5.

2. MLS APPROXIMATION SCHEME ON 3-D SURFACES

The MLS interpolation scheme for the RHBNM can be applied to a generic surface. Since the RHBNM nodes lie only on the boundary $\partial\Omega$ of a 3-D body Ω, the MLS approximation is needed on the bounding surfaces. It is assumed that, for 3-D problems, the bounding surface $\partial\Omega$ of a 3-D body is the union of piecewise smooth segments called panels. To avoid the discontinuity at edges and corners, the MLS interpolation is separately performed on each panel.

For the MLS interpolation on a generic surface, the first step is to choose a proper coordinate system. In CAD software models, surfaces are usually represented in parametric forms.

$$x = x(s_1, s_2), \quad y = y(s_1, s_2), \quad z = z(s_1, s_2)$$

where the parametric coordinates are defined in the range, $s_1, s_2 \in [0, 1]$. To be consistent with CAD software and render a general sense MLS scheme for all kinds of surface, the MLS interpolation on a surface are performed in the parametric plane as well. For problems in potential theory, the unknown potential function and its gradient on a surface are expressed in the parametric form as

$$u(x, y, z) = u(x(s_1, s_2), y(s_1, s_2), z(s_1, s_2)) = u(s_1, s_2)$$
$$q(x, y, z) \equiv \frac{\partial u}{\partial n} = q(x(s_1, s_2), y(s_1, s_2), z(s_1, s_2)) = q(s_1, s_2)$$

where n is a unit outward normal to $\partial\Omega$ at a point on it.

The MLS interpolation scheme will be coupled later with a 3-D hybrid "displacement" variational formulation that uses three independent variables, the potential and normal flux on the boundary and the potential inside the domain. Since the potential and the normal flux on the 2-D bounding surface will be interpolated by the MLS scheme, only $\tilde{u}$ and $\tilde{q}$ defined as the boundary potential and the normal flux will be addressed in this section.

For a panel over which a number of randomly located nodes $\{\mathbf{s}^I\}$, $I = 1, 2, \ldots, N$, the MLS interpolants for $\tilde{u}$ and $\tilde{q}$ are defined as

$$\tilde{u}(\mathbf{s}) = \sum_{j=1}^{m} p_j(\mathbf{s}) a_j(\mathbf{s}) = \mathbf{p}^{\mathbf{T}}(\mathbf{s})\mathbf{a}(\mathbf{s}) \tag{1}$$

$$\tilde{q}(\mathbf{s}) = \sum_{j=1}^{m} p_j(\mathbf{s}) b_j(\mathbf{s}) = \mathbf{p}^{\mathbf{T}}(\mathbf{s})\mathbf{b}(\mathbf{s}) \tag{2}$$

where $\mathbf{s}$ is a generic point with parametric coordinates (s_1, s_2), $p_1 = 1$ and $p_j(\mathbf{s})$, $j = 2, \ldots, m$ are monomials in (s_1, s_2). The monomials $p_j(\mathbf{s})$ provide the intrinsic polynomial bases for $\tilde{u}$ and $\tilde{q}$. In this study, a quadratic background basis is used, i.e.

$$\mathbf{p}^{\mathbf{T}}(\mathbf{s}) = \left[1, s_1, s_2, s_1^2, s_1 s_2, s_2^2\right], \quad m = 6 \tag{3}$$

The coefficient vector $\mathbf{a}(\mathbf{s})$ and $\mathbf{b}(\mathbf{s})$ is determined by minimizing a weighted discrete L_2 norm defined as

$$J_1(\mathbf{s}) = \sum_{I=1}^{N} w_I(\mathbf{s})[\mathbf{p}^{\mathbf{T}}(\mathbf{s}^I)\mathbf{a}(\mathbf{s}) - \hat{u}_I]^2 \tag{4}$$

$$J_2(\mathbf{s}) = \sum_{I=1}^{N} w_I(\mathbf{s})[\mathbf{p}^{\mathbf{T}}(\mathbf{s}^I)\mathbf{b}(\mathbf{s}) - \hat{q}_I]^2 \tag{5}$$

where points $\mathbf{s}^I$ are boundary nodes, $\mathbf{s}$ is an evaluation point E on the panel, N is the number of boundary nodes in the

neighborhood of E for which the weight functions $w_I(\mathbf{s}) > 0$. It should be noted here that $\hat{u}_I$ and $\hat{q}_I$, $I = 1, 2, \ldots, N$ are the fictitious nodal values other than the nodal values of the unknown $\tilde{u}_I$ and $\tilde{q}_I$ in general. This distinction between $\hat{u}_I$ and $\tilde{u}_I$ (or $\hat{q}_I$ and $\tilde{q}_I$) is very important in the view of the fact that MLS interpolants lack the delta function property.

Solving for $\mathbf{a}(\mathbf{s})$ and $\mathbf{b}(\mathbf{s})$ by minimizing J_1 and J_2 in equation (4) and (5), and substituting them into Eqs. (1) and (2), gives a relation that may be written as the form of an interpolation function similar to those used in the FEM, as

$$\tilde{u}(\mathbf{s}) = \sum_{I=1}^{N} \Phi_I(\mathbf{s})\hat{u}_I \tag{6}$$

$$\tilde{q}(\mathbf{s}) = \sum_{I=1}^{N} \Phi_I(\mathbf{s})\hat{q}_I \tag{7}$$

where

$$\Phi_I(\mathbf{s}) = \sum_{j=1}^{m} p_j(\mathbf{s})[A^{-1}(\mathbf{s})B(\mathbf{s})]_{jI} \tag{8}$$

with the matrices $A(\mathbf{s})$ and $B(\mathbf{s})$ defined by

$$A(\mathbf{s}) = \sum_{I=1}^{N} w_I(\mathbf{s})\mathbf{p}(\mathbf{s}^I)\mathbf{p}^{\mathbf{T}}(\mathbf{s}^I) \tag{9}$$

$$B(\mathbf{s}) = [w_1(\mathbf{s})\mathbf{p}(\mathbf{s}^1), w_2(\mathbf{s})\mathbf{p}(\mathbf{s}^2), \ldots, w_N(\mathbf{s})\mathbf{p}(\mathbf{s}^N)] \tag{10}$$

The MLS approximation is well defined only when the matrix A in Eq. (9) is non-singular.

The $\Phi_I(\mathbf{s})$ is usually called the shape function of the MLS approximation corresponding to nodal point $\mathbf{s}^I$. From Eqs. (8) and (10), $\Phi_I(\mathbf{s}) = 0$ when $w_I(\mathbf{s}) = 0$. The fact that $\Phi_I(\mathbf{s})$ vanishes for $\mathbf{s}$ not in the support of nodal point $\mathbf{s}^I$ preserves the local character of the MLS approximation.

Several kinds of weight function can be seen in the literature; the choice of weight functions and the consequences of a choice in the EFG method are discussed in some detail elsewhere [14]. In this study, Gaussian weight function is selected. Corresponding to a node $\mathbf{s}^I$, the Gaussian weight function may be written as

$$w_I(\mathbf{s}) = \begin{cases} \dfrac{\exp[-(d_I/c_I)^2] - \exp[-(\hat{d}_I/c_I)^2]}{1 - \exp[-(\hat{d}_I/c_I)^2]}, & 0 \le d_I \le \hat{d}_I \\ 0, & d_I \ge \hat{d}_I \end{cases} \tag{11}$$

where c_I is a constant controlling the shape of the weight function, and $\hat{d}_I$ is the size of the support for the weight function w_I. From Eq. (10), the weight function has compact support, which is decided by the parameter $\hat{d}_I$. The compact support is also an associated range of influence for each node. Usually, the shape of the compact support is chosen to be a circle in meshless models. Because a circle becomes an ellipse when mapped from real space into parametric space, this study used an ellipse for the shape of the compact support with $\hat{d}_I$ being the half-length of major axis of the ellipse. Denoting the half-length of minor axis by $\hat{d}'_I$, then

$$d_I = \sqrt{\left(s_1 - s_1^I\right)^2 + \frac{\hat{d}_I^2}{\hat{d}_I'^2}\left(s_2 - s_2^I\right)^2}$$

The $\hat{d}_I$ and $\hat{d}'_I$ should be chosen such that they should be large enough to have sufficient number of nodes covered in the domain of definition of every sample point ($N \ge m$) to ensure the regularity of A. But too large $\hat{d}_I$ and $\hat{d}'_I$ will lose the local character of the MLS interpolation, or even leads to ill-conditioned matrix A [15]. In this study, $\hat{d}_I$ and $\hat{d}'_I$ are chosen such that $2\,m \sim 4\,m$ nodes are included in the support of each node.

3. REGULAR HYBRID BOUNDARY NODE METHOD

The potential problem in three dimensions governed by Laplace's equation with boundary conditions is written as

$$\begin{aligned} &u_{,ii} = 0, && \forall x \in \Omega \\ &u = \bar{u}, && \forall x \in \Gamma_u \\ &u_{,i}\, n_i \equiv q = \bar{q}, && \forall x \in \Gamma_q \end{aligned} \tag{12}$$

where the domain Ω is enclosed by $\Gamma = \Gamma_u + \Gamma_q$, $\bar{u}$ and $\bar{q}$ are the prescribed potential and normal flux, respectively, on the essential boundary Γ_u and on the flux boundary Γ_q, and n is the outward normal direction to the boundary Γ, with n_i components.

The RHBNM is based on a modified variational principle. The independent functions are assumed to be

- potential field in the domain, u;
- boundary potential field, $\tilde{u}$;
- boundary normal flux, $\tilde{q}$.

The corresponding variational functional Π_{AB} is defined as

$$\Pi_{AB} = \int_\Omega \frac{1}{2} u_{,i}\, u_{,i}\, d\Omega - \int_\Gamma \tilde{q}(u - \tilde{u}) d\Gamma - \int_{\Gamma_q} \bar{q}\tilde{u} d\Gamma \tag{13}$$

where the boundary potential $\tilde{u}$ satisfies the essential boundary condition, i.e., $\tilde{u} = \bar{u}$ on Γ_u.

By carrying out the variations it can be shown that

$$\begin{aligned} \delta\Pi_{AB} = &\int_\Gamma (q - \tilde{q})\delta u d\Gamma - \int_\Omega u_{,ii}\,\delta u d\Omega \\ &+ \int_{\Gamma_q} (\tilde{q} - \bar{q})\delta\tilde{u} d\Gamma - \int_\Gamma (u - \tilde{u})\delta\tilde{q} d\Gamma \end{aligned} \tag{14}$$

The vanishing of $\delta\Pi_{AB}$ for arbitrary variations δu in Ω, $\delta\tilde{u}$ and

$\delta\tilde{q}$ on Γ, with $\delta\tilde{u} = 0$ on Γ_u, gives the following Euler equations:

$$\begin{aligned} u_{,ii} &= 0, \quad \text{in } \Omega \\ u - \tilde{u} &= 0, \quad \text{on } \Gamma \\ q - \tilde{q} &= 0, \quad \text{on } \Gamma \\ \tilde{q} - \bar{q} &= 0, \quad \text{on } \Gamma_q \end{aligned} \tag{15}$$

Consequently, the solution of the problem is now given in terms of the functions u, $\tilde{u}$ and $\tilde{q}$, which makes $\delta\Pi_{AB}$ stationary.

With the vanishing of $\delta\Pi_{AB}$, we have the following equivalent integral equations:

$$\int_\Gamma (q - \tilde{q})\delta u d\Gamma - \int_\Omega u_{,ii}\,\delta u d\Omega = 0 \tag{16}$$

$$\int_\Gamma (u - \tilde{u})\delta\tilde{q} d\Gamma = 0 \tag{17}$$

$$\int_{\Gamma_q} (\tilde{q} - \bar{q})\delta\tilde{u} d\Gamma = 0 \tag{18}$$

If the flux boundary condition, $\tilde{q} = \bar{q}$, is imposed in the same way as the essential boundary condition after the matrices have been computed, Eq. (18) holds. So it can be ignored temporarily in the following development.

Equations (16) and (17) hold in any sub-domain, for example, in a sub-domain Ω_s and its boundary Γ_s and L_s (see Figure 1). Following Zhu [16], the following weak forms are used for the sub-domain Ω_s and its boundary Γ_s and L_s to replace Eqs. (16) and (17):

$$\int_{\Gamma_s + L_s} (q - \tilde{q})v d\Gamma - \int_{\Omega_s} u_{,ii}\, v d\Omega = 0 \tag{19}$$

$$\int_{\Gamma_s + L_s} (u - \tilde{u})v d\Gamma = 0 \tag{20}$$

where v is a test function. Equations (19) and (20) hold irrespective of the size and the shape of Ω_s and its boundary $\partial\Omega_s$. This is an important observation, which forms the basis for the following development. We now deliberately choose a simple regular shape for Ω_s. The most regular shape of a sub-domain should be an n-dimensional sphere for a boundary value problem defined on an n-dimensional space. In the present paper, the sub-domain Ω_s is chosen as the intersection of the domain Ω and a sphere centered at a boundary node $\mathbf{s}_J$ (see Figure 1).

In Eqs. (19) and (20), $\tilde{u}$ and $\tilde{q}$ on Γ_s are interpolated by MLS in Eqs. (6) and (7), but on L_s, they have not been defined yet. To solve this problem, we deliberately select v such that all integrals over L_s vanish. This can be easily accomplished by choosing v as the weight function in the MLS approximation, with the half-length of the major axis $\hat{d}_I$ replaced by the radius r_J of the sub-domain Ω_s, namely

$$v_J(Q) = \begin{cases} \dfrac{\exp[-(d_J/c_J)^2] - \exp[-(r_J/c_J)^2]}{1 - \exp[-(r_J/c_J)^2]}, & 0 \le d_J \le r_J \\ 0, & d_J \ge r_J \end{cases} \tag{21}$$

where d_J is the distance between a domain point Q and the nodal point $\mathbf{s}_J$. Therefore, v vanishes on L_s.

The u and q in Ω and on Γ are defined as

$$u = \sum_{I=1}^{NN} U_I x_I \tag{22}$$

$$q = \sum_{I=1}^{NN} \frac{\partial U_I}{\partial n} x_I \tag{23}$$

where U_I is the fundamental solution of Lapalce's equation ; x_I are unknown parameters; NN is the total number of boundary nodes.

For 3-D potential problem, the fundamental solution is

$$U_I = \frac{1}{4\pi}\frac{1}{r(Q, P_I)} \tag{24}$$

where Q and P_I are the field point and the source point respectively. P_I is outside the domain and determined by

$$P_I = \mathbf{s}^I + \mathbf{n}(\mathbf{s}^I) \cdot h \cdot SF \tag{25}$$

where h is the average distance between neighboring nodes, $\mathbf{n}(\mathbf{s}^I)$ is the unit outward normal to the boundary at node $\mathbf{s}^I$, and

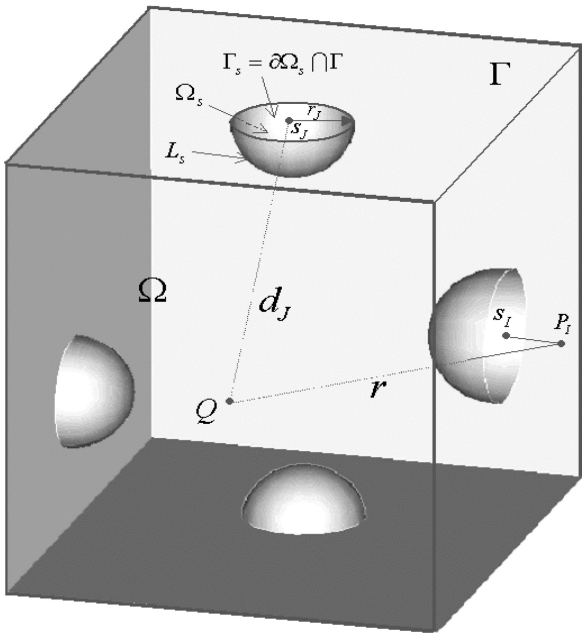

FIG. 1. The local domain centered at a node s_J and the source point of fundamental solution corresponding to a node s_I.

SF is a scale factor. As can be imagined, the scale factor, *SF*, plays an important role in the performance of the present method. Too small a value for *SF* will lead to nearly singular integrals and thus inaccurate results. On the other hand, too large a value will lead to an ill-conditioned system of algebraic equations as well. From our computations, the proper range for *SF* is between 3.0 and 6.0.

As u is expressed by Eq. (22), the last term at the left-hand side of Eq. (19) vanishes. Substituting Eqs. (6), (7), (21), (22) and (23) into Eqs. (19) and (20), and omitting the vanished terms, we have

$$\begin{aligned}\sum_{I=1}^{n}\int_{\Gamma_s}\frac{\partial U_I}{\partial n}v_J(Q)x_I d\Gamma &= \sum_{I=1}^{n}\int_{\Gamma_s}\Phi_I(\mathbf{s})v_J(Q)\hat{q}_I d\Gamma\\ \sum_{I=1}^{n}\int_{\Gamma_s}U_I v_J(Q)x_I d\Gamma &= \sum_{I=1}^{n}\int_{\Gamma_s}\Phi_I(\mathbf{s})v_J(Q)\hat{u}_I d\Gamma\end{aligned} \tag{26}$$

Writing the above equations for all nodes, we obtain the following system of equations:

$$\mathbf{U}\mathbf{x} = \mathbf{H}\hat{\mathbf{q}} \tag{27}$$

$$\mathbf{V}\mathbf{x} = \mathbf{H}\hat{\mathbf{u}} \tag{28}$$

where

$$\begin{aligned}U_{IJ} &= \int_{\Gamma_s^J}\frac{\partial U_I}{\partial n}v_J(Q)d\Gamma\\ V_{IJ} &= \int_{\Gamma_s^J}U_I v_J(Q)d\Gamma\\ H_{IJ} &= \int_{\Gamma_s^J}\Phi_I(\mathbf{s})v_J(Q)d\Gamma\\ \mathbf{x}^{\mathrm{T}} &= [x_1, x_2, \cdots, x_n]\\ \hat{\mathbf{q}}^{\mathrm{T}} &= [\hat{q}_1, \hat{q}_2, \ldots, \hat{q}_n]\\ \hat{\mathbf{u}}^{\mathrm{T}} &= [\hat{u}_1, \hat{u}_2, \ldots, \hat{u}_n]\end{aligned}$$

The evaluation of the matrices $\mathbf{U}$ and $\mathbf{V}$ is much simpler than that in BEM and BNM. No singular integration is involved, as the source points of fundamental solutions determined by equations (25) are outside the domain.

For well-posed problems, either u or q is known at each node on the boundary. However, transformations between $\hat{u}_I$ and $\tilde{u}_I$, $\hat{q}_I$ and $\tilde{q}_I$ must be performed due to the fact that the MLS interpolants lack the delta function property of the usual BEM shape functions [17, 18]. For u prescribed panels, $\hat{u}_I$ can be obtained by

$$\hat{u}_I = \sum_{J=1}^{N}R_{IJ}\tilde{u}_J = \sum_{J=1}^{N}R_{IJ}\bar{u}_J \tag{29}$$

and for q prescribed panels, $\hat{q}_I$ can be obtained by

$$\hat{q}_I = \sum_{J=1}^{N}R_{IJ}\tilde{q}_J = \sum_{J=1}^{N}R_{IJ}\bar{q}_J \tag{30}$$

where $R_{IJ} = [\Phi_J(\mathbf{s}^I)]^{-1}\circ$ Rearranging Eqs. (27) and (28) gives the final system of equations to uniquely determine $\mathbf{x}$.

The potential u and the flux q at any point inside domain Ω or on boundary Γ are evaluated by Eqs. (22) and (23) without further integrations. Since u and q on boundary Γ can be evaluated in the same way as those inside domain, the unknowns $\hat{\mathbf{q}}$ and $\hat{\mathbf{u}}$ need not be computed and hence the evaluation of inverse matrix $\mathbf{V}^{-1}$ is avoided. This is in contrast to that in the Hybrid BNM [7].

As can be seen, the present method is truly meshless with no boundary elements used for interpolations or for integrations. Moreover, no further integration is needed in the "post-processing" step.

4. ILLUSTRATIVE NUMERICAL RESULTS

A few illustrative numerical results from the RHBNM, together with comparisons with exact solutions, follow. In all cases, the Laplace equation $\nabla^2 u = 0$ is solved with appropriate prescribed boundary conditions. In the present method, the MLS interpolation and the local surface integration are performed separately. Therefore, the MLS points $\mathbf{s}^I$ in Eqs. (9) and (10) also independent of the nodes $\mathbf{s}^J$ in Eq. (25). Computations show that the relative locations of the MLS points $\mathbf{s}^I$ and the nodes $\mathbf{s}^J$ have no effect on the numerical results. This is in contrast to that in the BNM [15].

For the purpose of error estimation and convergence studies, a "global" L_2 norm error, normalized by $|u|_{\max}$ is defined as

$$e = \frac{1}{|u|_{\max}}\sqrt{\frac{1}{N}\sum_{i=1}^{N}\left(u_i^{(e)} - u_i^{(n)}\right)^2} \tag{31}$$

where $|u|_{\max}$ is the maximum value of u over N sample points, the superscripts (e) and (n) refer to the exact and numerical solutions, respectively.

The method has been tested thoroughly on three 3-D geometrical objects, namely the sphere, the cube and the elbow hose. To compare the current method with the BNM, the first two are taken from reference [15]. And the last one is added to show the advantage of the truly meshless nature of the current method.

The following issues have been investigated:

(i) the scale factor, *SF*, in Eq. (25),
(ii) the radius r_J of the local sub-domain in Eq. (21).

In all examples, if not mentioned, the size of support for weight function, $\hat{d}_I$ in Eq. (11), is taken to be $3.0h$, and c_I be such that $\hat{d}_I/c_I$ is constant and equal to 3.0. The size of the local

domain (radius r_J) for each node is chosen as 1.5 h and c_I in Eq. (21) taken to be such that r_J/c_J is constant and equal to 3.0. To perform the integration in Eq. (26), all local surfaces Γ_s are mapped into unit circles in the parametric space, and a unit circle is divided into 8 parts, 2 segments in radial and 4 segments in circumference, respectively. In each part, 5×5 Gauss points are used.

4.1. Dirichlet Problem on a Sphere

The example solved here is the Laplace's equation on a sphere of radius 2 centered at the origin. The usual spherical polar coordinates θ and ϕ are used. On the surface, 800 MLS points and 136 uniformly spaced nodes are used. Three cases are tested, in which the exact solution are as follows, respectively:

(i) Linear solution

$$u = x + y + z \tag{32}$$

(ii) Quadratic solution

$$u = xy + yz + zx \tag{33}$$

(iii) Cubic solution

$$u = x^3 + y^3 + z^3 - 3yx^2 - 3xz^2 - 3zy^2 \tag{34}$$

In each case, the Dirichlet boundary conditions corresponding to the exact solutions have been imposed on the surface of the sphere. The relative errors (Eq. (31)) of u and its x-derivative inside the sphere, denoted by DM-u and DM-q in the figures, are evaluated over 11 sample points uniformly distributed from (0,0,0) to (2,0,0); and the relative errors of u and $q(\equiv \partial u/\partial n)$ on the surface, denoted by SF-u and SF-q in the figures, are evaluated over 11 sample points uniformly distributed along the half equator of the sphere ($0 \leq \theta \leq \pi$). Results for various sub-domain radius, r_J, are shown in Figure 2. It should be noted here that the $\cup\Gamma_s$ do not cover the whole bounding surface when $r_J \leq 0.5\,h$ (where h is the mesh size), and the Γ_s will be overlapped when $r_J \geq h$. Figure 2 shows that results are in all cases accurate no matter whether Γ_s are overlapped, or even uncover the body's boundary.

The scale factor *SF* in Eq. (25) is also studied in this example. Figure 3 shows the relative errors as a function of *SF*. Results are very accurate for $SF \geq 2.0$. As mentioned earlier, a too-large value of *SF* may lead to an ill-conditioned system of equation. Further study shows that the largest value of *SF* that ensure the RHBNM non-degenerate is 26.0, and this value is independent of boundary conditions while dependent on the domain geometry and meshing.

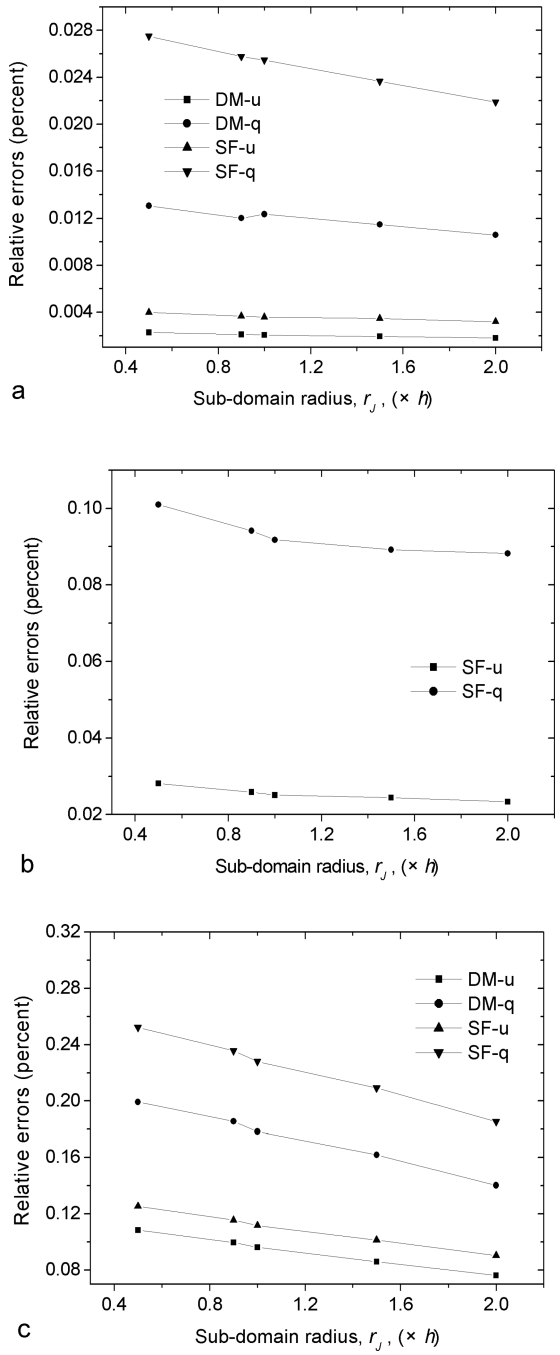

FIG. 2. Relative errors for various sub-domain radius, r_J: **a** for the linear field, **b** for quadratic the field, **c** for the cubic field.

A more challenging problem has also been tested, in which the following analytical solution is used

$$u = \frac{2r^2}{R^2}\cos^2\phi - \frac{2r^2}{3R^2} - \frac{1}{3} \tag{35}$$

where R is the radius of the sphere and ϕ the angle measured from the z-axis. The Dirichlet boundary condition on the surface

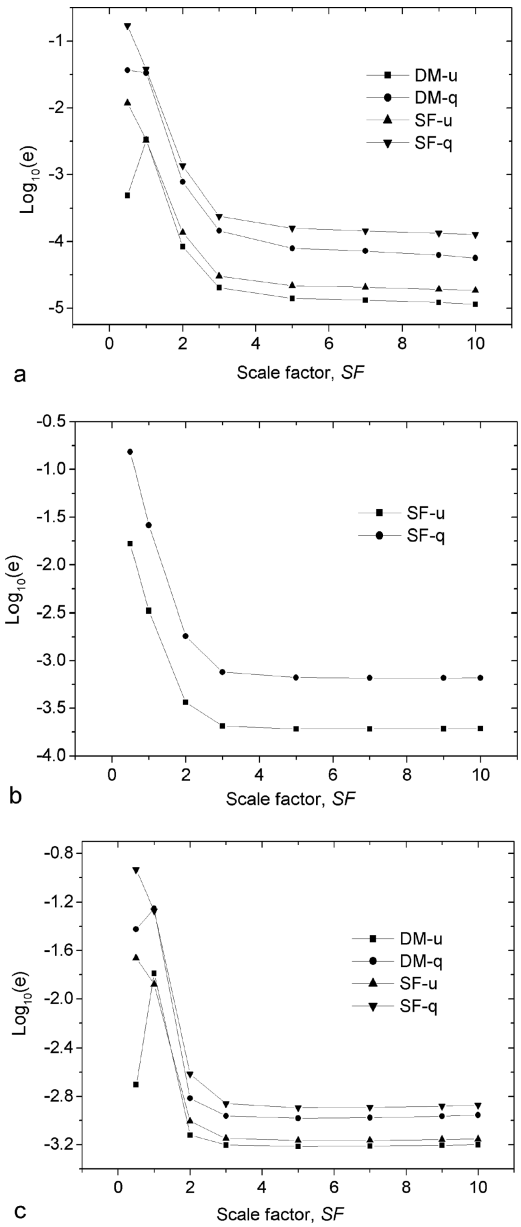

FIG. 3. Relative errors for various scale factors, *SF*: **a** for the linear field, **b** for quadratic the field, **c** for the cubic field.

then becomes

$$u|_{(r=R)} = \cos 2\phi \tag{36}$$

Numerical results show that the relative errors for u and q on the surface are 0.0117 and 0.0439, respectively, for $r_J = 1.5h$ and $SF = 3.0$. The u and q along the meridian from the RHBNM are shown in Figure 4 with exact solutions. In the RHBNM, it is very appealing that very high accuracy can be achieved. The numerical results almost reproduce the analytical solution exactly, and are no more sensitive to the proximity of the interior points to the boundary, in contrast with that in the Hybrid BNM [7] or other hybrid boundary element methods [12].

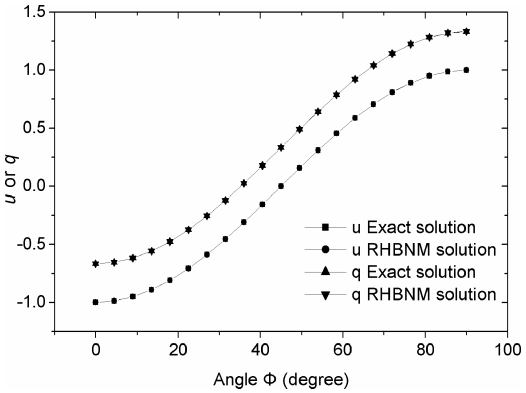

FIG. 4. u and q along the meridian of the sphere.

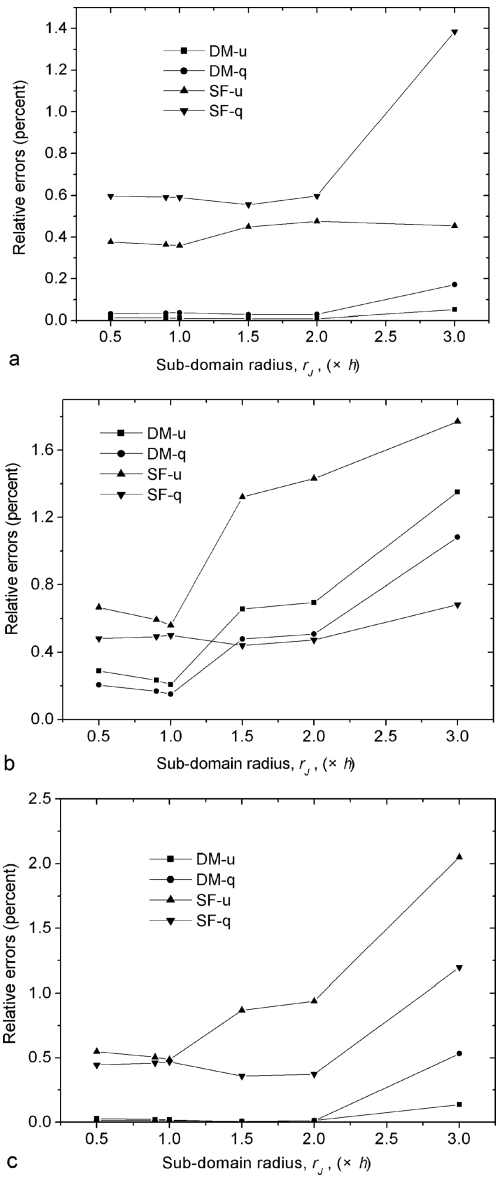

FIG. 5. Relative errors for various sub-domain radius, r_J: **a** for Dirichlet problem, **b** for Neumann problem, **c** for mixed problem.

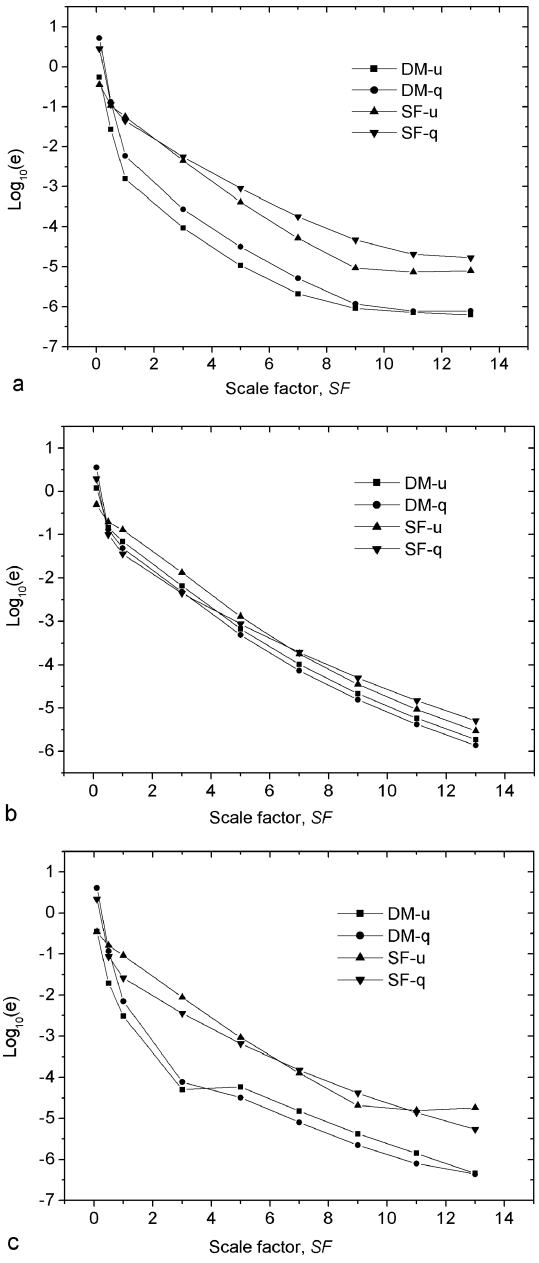

FIG. 6. Relative errors for various scale factor, *SF*: **a** for Dirichlet problem, **b** for Neumann problem, **c** for mixed problem.

4.2. Dirichlet, Neumann and Mixed Problem on a Cube

The second example considers a cube that is bounded by the surfaces $x = \pm 1$, $y = \pm 1$ and $z = \pm 1$. Equation (34) is used as the exact solution. A Dirichlet problem and a Neumann problem are solved for which the essential boundary condition and the natural boundary condition are prescribed on all faces, corresponding to the exact solution, respectively, and a mixed problem for which the essential boundary condition is imposed on faces $z = \pm 1$, and the natural boundary condition on faces $x = \pm 1$ and $y = \pm 1$. 10×10 MLS points and 5×5 nodes on each face are used.

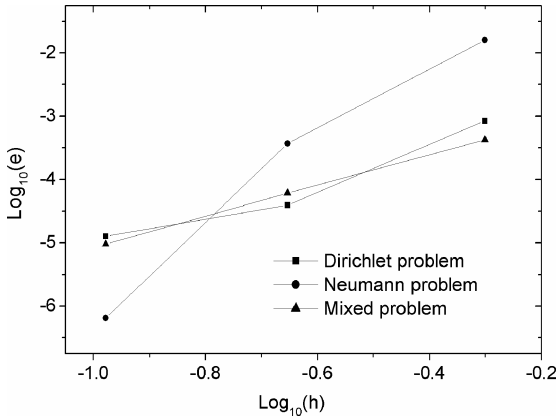

FIG. 7. Relative errors and convergence rates for Dirichlet, Neumann and mixed problem on a cube.

The relative errors of u and its x-derivative inside the cube, denoted by DM-u and DM-q in the figures, are evaluated by Eq. (31) over 11 sample points uniformly distributed from (0,0,0) to (1,0,0); and that on the surface, denoted by SF-u and SF-q in the figures, are evaluated over 11 sample points uniformly distributed on the diagonal of the face $x = 1$. Results for various sub-domain radius, r_J, with $SF = 3.0$, for the Dirichlet, Neumann and mixed problems are shown in Figure 5. It can be seen that results are accurate in all cases no matter whether Γ_s are overlapped, or even uncover the entire boundary.

The effect of the selection of the scale factor *SF* has also been studied in this example. Figure 6 shows that results are all accurate when $SF \geq 2.0$. As mentioned earlier, the scale factor *SF* cannot be too large. Fortunately, from Figure 6, it is easy to see that we have a wide range to choose a proper value for *SF* in the case that the RHBNM does not degenerate.

To study the convergence of the present method, the Dirichlet, Neumann and mixed problems have been tested on three regular nodes arrangements: (a) 5×5 nodes on each face, (b) 10×10 nodes on each face, and (c) 20×20 nodes on each face, with $SF \times h$ to be constant and equal to 1.0. Figure 7 shows the

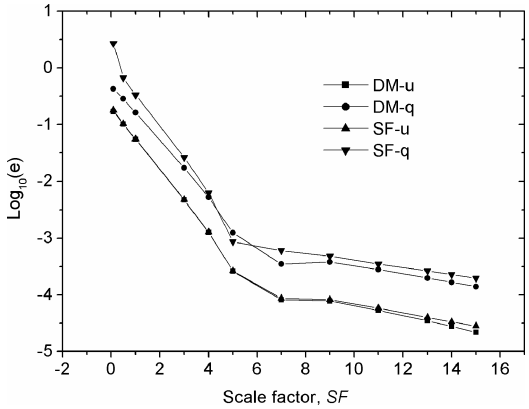

FIG. 8. Relative errors for various scale factor, *SF*, for Dirichlet problem on a cube with a complicated field.

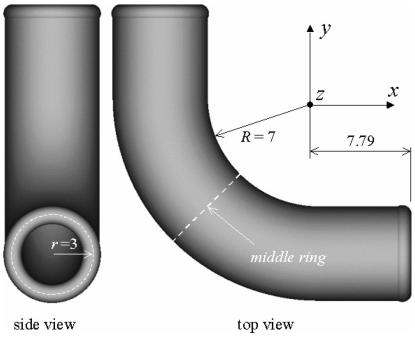

FIG. 9. The elbow pipe and its main sizes.

convergence of the x-derivate inside the cube. It can be seen that the present RHBNM has high rates of convergence.

In addition to the polynomial representations of the exact solution, a problem has been tried with the following exact solution:

$$u = \sinh \frac{\pi x}{2} \sin \frac{\pi y}{2\sqrt{2}} \sin \frac{\pi z}{2\sqrt{2}} \tag{37}$$

Dirichlet boundary conditions according the exact solution are imposed on the surface of the cube. Again, 10×10 MLS points and 5×5 nodes on each face are used. The relative errors for various SF with $r_J = 1.5h$ are shown in Figure 8. It is appealing that the results are most accurate when $SF \geq 2.0$.

4.3. Dirichlet Problem on an Elbow Pipe

In order to show the advantages of the truly meshless nature of the RHBNM, a more complicated geometry, namely an elbow pipe, is considered here, which is shown in Figure 9 with main dimensions. Three analytical fields, namely linear field (Eq. (32)), quadratic field (Eq. (33)) and cubic field (Eq. (34)), have been considered. In all cases, Dirichlet boundary conditions are imposed on the entire boundary, and 1500 MLS points and 1250 nodes are used with r_J =1.5 and SF=1.0. The relative errors of u and x-derivate inside the domain, evaluated on 11 sample points uniformly spaced on a internal line segment from (0,7.5,0) to (5,7.5,0), are 0.02303% and 0.1034% for the linear field, 0.0178% and 0.144% for the quadratic field, and 0.09126% and 0.164% for the cubic field, respectively. The relative errors of q evaluated over 31 sample points along the middle ring (see Figure 9), are 1.421%, 1.136% and 1.276% for the linear, quadratic and cubic fields, respectively. Numerical results of q along the middle ring, together with the exact solution, are shown in Figure 10. The numerical results agree excellently with the exact solutions again. It should be pointed out here that the input file for this problem contains only 263 data! The RHBNM, if anything, is somewhat flexible and convenient, and is an important step toward complete analysis automation.

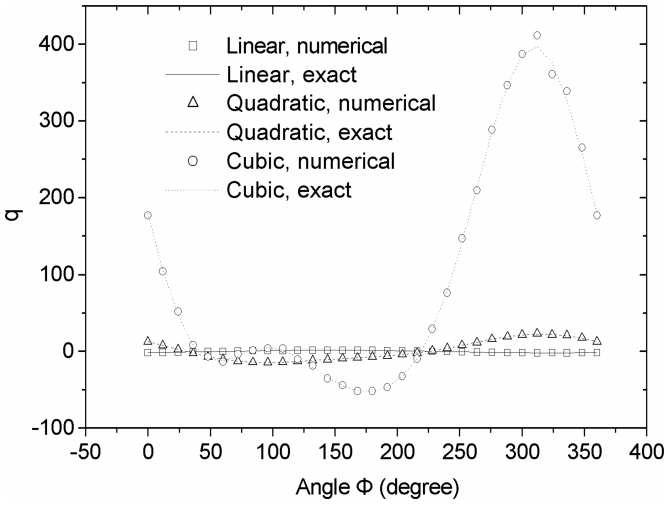

FIG. 10. Normal flux, q, along the middle ring of the elbow pipe.

5. CONCLUSIONS AND DISCUSSION

The regular hybrid boundary node method has been extended to solve potential problems in three dimensions. The RHBNM is based on a hybrid model that involves three types of independent variables, i.e. potentials and normal fluxes on the boundary and potentials inside the domain, and coupled with the MLS interpolation scheme over the boundary variables. Compared with the MLBIE and MLPG, the RHBNM has the well-known dimensionality of the BEM, e.g. for a 3-D object, only the 2-D bounding surface needing be discretized. Compared with the conventional BEM, it is a meshless method, requiring only a nodal data structure on the bounding surface. Compared with the BNM, it is a truly meshless method, with absolutely no cells needed either for interpolation or integration purposes.

Numerical examples have shown the accuracy and convergence of the method. The solution is most accurate for the potentials and fluxes on the boundary and in the domain. High rates of convergence have been achieved.

In contrast with the conventional BEM, reduced to the solution of the singular-integral equations of the second kind, the RHBNM leads to regular-integral equation of the first kind. The evaluation of variables at internal points needs not further integration. As no singularities are involved, the serious "boundary layer effect" that appears in the Hybrid BNM is eliminated.

However, the outside assignment of the source points of the fundamental solutions causes some new problems. The performance of the method is dependent on the value of the scale factor, SF. Moreover, it is usually difficult to locate the source points when a domain with concave boundary is considered. In this study, the scale factor is only empirically determined by numerical experiments, just as the other constant parameters in Eqs. (11) and (21). For problems with concave boundary, the multi-domain approach is recommended.

Although some drawbacks exist, e.g. many constant parameters have to be determined by experience, the advantages of the

RHBNM, such as meshless nature, high accuracy, high convergence rate and no singularities, etc., are so attractive that this method is certainly worthy of attention.

REFERENCES

1. L.B. Lucy, A Numerical Approach to the Testing of the Fission Hypothesis, Astronomy Journal, vol. 8, pp. 1013–1024, 1977.
2. B. Nayroles, G. Touzot, P. Villon, Generalizing the Finite Element Method: Diffuse Approximation and Diffuse Element, Comput. Mech., vol. 10, pp. 307–318, 1992.
3. T. Belytchko, Y.Y. Lu, L. Gu, Element Free Galerkin Methods, Int. J. Numer. Meth. Engng., vol. 37, pp. 229–256, 1994.
4. T. Zhu, J. Zhang, S.N. Atluri, A Local Boundary Integral Equation (LBIE) Method in Computation Mechanics, and a Meshless Discretization Approach, Comput. Mech., vol. 21, pp. 223–235, 1998.
5. S.N. Atluri, T. Zhu, A New Meshless Local Petrov-Galerkin Approach in Computational Mechanics, Comput. Mech., vol. 22, pp. 117–127, 1998.
6. Y.X. Mukherjee, S. Mukherjee, The Boundary Node Method for Potential Problems, Int. J. Numer. Meth. Engng., vol. 40, pp. 797–815, 1997.
7. J.M. Zhang, Z.H. Yao, H. Li, A Hybrid Boundary Node Method, Int. J. Numer. Meth. Engng., vol. 53, pp. 751–763, 2002.
8. J.M. Zhang, Z.H. Yao, Meshless Regular Hybrid Boundary Node Method, Computer Modeling in Engineering & Sciences, vol. 2, pp. 307–318, 2001.
9. J.M. Zhang, Z.H. Yao, The Meshless Regular Hybrid Boundary Node Method for 2-D Linear Elasticity, Engineering Analysis with Boundary Elements, vol. 27, pp. 259–268, 2003.
10. J.M. Zhang, Z.H. Yao, Analysis of 2-D Thin Structures by the Meshless Regular Hybrid Boundary Node Method, Acta Mechanica Solida Sinica, vol. 15, pp. 36–44, 2002.
11. N.A. Dumount, The Hybrid Boundary Element Method, Proc. 9th Int. Conf. on BEM. Stuttgart, Computational Mechanics Publications, Southampton, 1987.
12. T.G.B. DeFigueredo, C.A. Brebbia, A New Hybrid Displacement Variational Formulation of BEM for Elastostatics, in C.A. Brebbia and J.J. Conner (eds.), Advances in Boundary Elements, Computational Mechanics Publications, vol. 1, pp. 47–57, 1989.
13. E. Schnack, A Hybrid BEM Model, Int. J. Numer. Meth. Engng., vol. 24, pp. 1015–1025, 1987.
14. T. Belytchko, Y. Krongauz, D. Organ, M. Fleming, P. Krysl, Meshless Methods: An Overview and Recent Developments, Comput. Meth. Appl. Mech. Engng., vol. 139, pp, 3–47, 1996.
15. M.K. Chati, S. Mukherjee, The Boundary Node Method for Three-dimensional Problems in Potential Theory, Int. J. Numer. Meth. Engng., vol. 47, pp. 1523–1547, 2000.
16. T. Zhu, A New Meshless Regular Local Boundary Integral equation (MRLBIE) Approach, Int. J. Numer. Meth. Engng., vol. 46, pp.1237–1252, 1999.
17. S.N. Atluri, H.G. Kim, J.Y. Cho, A Critical Assessment of the Truly Meshless Local Petrov-Galerkin (MLPG), and Local Boundary Integral Equation (LBIE) Methods, Comput. Mech., vol. 24, pp. 348–372, 1999.
18. T.-L. Zhu, J. Zhang, D. Wang , A Meshless Local Petrov-Galerkin (MLPG) Approach Based on the Regular Local Boundary Integral Equation for Linear Elasticity, International Journal for Computational Methods in Engineering Science and Mechanics, vol. 8, no. 5, pp. 373–382, 2007.